

Surface modifications induced by ns and sub-ps excimer laser pulses on titanium implant material

M. Bereznai^{a,*}, I. Pelsöczy^b, Z. Tóth^c, K. Turzó^b, M. Radnai^b, Z. Bor^a, A. Fazekas^b

^a Department of Optics and Quantum Electronics, University of Szeged, Dóm tér 9., Szeged, H-6720, Hungary

^b Department of Dentistry and Oral Surgery, University of Szeged, Tisza Lajos krt. 64., Szeged, H-6720, Hungary

^c Research Group on Laser Physics, Hungarian Academy of Sciences, Dóm tér 9., Szeged, H-6720, Hungary

Received 21 December 2002; accepted 8 April 2003

Abstract

Medical implants used in oral and orthopaedic surgery are mainly produced from titanium. Their biological behaviour, e.g. osseointegration, essentially depends on both the chemical composition and the morphology of the surface. Modifications achieved by excimer laser irradiation of titanium samples were investigated in order to improve their surface characteristics so as to facilitate biointegration. To enlarge the effective interfacial area of bone–implant contact, holes were ablated by laser pulses of ns or sub-ps length. During ns ablation, crown-like projecting rims formed around the borders of the holes. Ultra-short (0.5 ps) KrF excimer laser pulses were successfully applied to avoid these undesirable formations. Since a smooth dental implant surface is necessary to maintain a healthy connection with the soft tissues, laser polishing of samples was investigated, too. Irradiation with a series of ns laser pulses resulted in effective smoothing, as measured with atomic force microscope. X-ray photoelectron spectroscopy analysis of the laser-polished titanium surface revealed that laser treatment led to a decrease of the surface contamination and in thickening of the oxide layer. X-ray diffraction measurements demonstrated that the original α -titanium crystal structure was preserved.

© 2003 Elsevier Science Ltd. All rights reserved.

Keywords: Titanium; Osseointegration; Laser ablation; Surface modification; Surface roughness

1. Introduction

Dental implants are frequently applied to replace lost teeth. A wide variety of materials have been used to produce endosseous implants [1–3]. Titanium and its alloys are currently the most commonly used dental and orthopaedic implant materials, meeting the most important requirements [4–6]. The properties of titanium and of its surface, which is covered by a native oxide layer, are appropriate to allow its use as a biocompatible material [7,8].

The long-term benefits of dental implants depend on the responses of the different surrounding host tissues (the alveolar bone, the conjunctival part of the oral soft tissues and the gingival epithelium). As regards osseointegration, i.e. the formation of a direct connection between the living bone and the surface of load-carrying

implants, the important question arises as to how to attain better integration by modification of the implant surface morphology. Many authors have suggested that the surface should be free from any contamination [9–12]. Another important property of the implant surface is its morphology [13]. The mechanical roughness of the implant surface plays a significant role in anchoring cells and connecting together the surrounding tissues, thereby leading to a shorter healing period. The area of contact can be enlarged by microstructuring the implant surface. Rough titanium surfaces display advantages over smooth ones, e.g. a shorter bone-healing period [14–17].

The presence of a healthy gingival attachment on an implant is also influenced by the surface characteristics [18]. Connective tissues surrounding dental implants do not become directly attached to the implant surface, but merely adhere to it. For bioinert and bioactive implant materials, a glycoprotein layer ensures the connection of the collagen fibres to the implant surface. Although a rough surface would be favourable for the epithelial

*Corresponding author. Tel.: +36-62-544-653; fax: +36-62-544-658.

E-mail address: bereznai@physx.u-szeged.hu (M. Bereznai).

attachment, the neck part of an implant has to be polished in order to avoid pathogenic plaque accumulation [19].

To increase the roughness of solid surfaces, a number of laser-based techniques have been applied in recent years [20]. Besides the prompt intense heating of the surface, excimer laser illumination may further enhance the sterilising effect in consequence of the high dose in the UV range.

Recent studies on the laser machining of dental implants revealed that an appropriate structure with the least contamination could be achieved by means of laser treatment [21,22]. After multipulse irradiation with a focused Nd:YAG laser beam, a crown-like structure formation was observed on the titanium surface [23]. The efficient oxidation of titanium through Nd:YAG laser irradiation was reported in [24,25]. The importance of these results lies in the fact that they involve laser technologies for the processing of implant surfaces which already have numerous industrial applications. However, these techniques must be further improved, since medical applications require high accuracy in both mechanical and chemical characteristics.

The aim of the present study was to obtain results relating to excimer laser modifications, such as the polishing and structuring of titanium surfaces. The thickness of the oxide layer and the changes in the oxidation states of the laser-polished surface were investigated by means of X-ray photoelectron spectroscopy (XPS). Structural changes caused in the crystalline structure by rapid laser annealing were examined by X-ray diffraction (XRD) measurements. Optical microscopy, scanning electron microscopy (SEM) and atomic force microscopy (AFM) was applied to visualise the surface structures formed by local excimer laser ablation.

2. Material and methods

2.1. Titanium samples

Titanium sample discs 1.25 mm thick and 8 mm in diameter were cut from commercially pure titanium rods (CP grade 1, <0.12% O, <0.05% N, <0.06% C, <0.013% H), used for the fabrication of dental implants. Concentric scratches 0.1–2 μm in depth were observable on the surface of the machined samples. Before laser treatment, all samples were cleaned ultrasonically in a distilled water–detergent mixture, and then rinsed in pure distilled water and finally in absolute ethanol.

2.2. Surface polishing with a ns ArF excimer laser

An ArF excimer laser (Lambda Physics EMG 201, wavelength: 193 nm, pulse duration: 18 ns, pulse energy:

100 mJ) was used for polishing. A square aperture that cut out the most homogeneous part of the beam was imaged onto the surface of the samples by a fused silica lens ($f = 5$ cm). A 3.6 mm² area on the sample disc was illuminated by different series of laser pulses under atmospheric conditions. The fluence at the sample was monitored by calibrated energy measurement of a reference beam, coupled out by a fused silica plate.

In the experiments concerning laser polishing, two parameters were varied independently: the incident fluence was varied in the range 1.5–5 J/cm² by placing neutral filters in the beam path, and experiments were performed with 10, 100 or 1000 shots of excimer pulses.

2.3. Microstructuring

2.3.1. Nanosecond ArF excimer laser ablation

For the local ablation of titanium surfaces, a similar set-up was used as in the case of the laser polishing experiments. A copper grid was placed in the beam path and its rectangular holes (0.29 mm² in area) were imaged by a fused silica lens with a focal length of 4 cm onto the sample surface. In this case a greater reduction of the beam was applied, and therefore the local average fluence was higher: 8.5 J/cm². 250, 500 and 1000 pulses were shot for local ablation experiments.

2.3.2. Laser ablation with 0.5 ps KrF excimer pulses

Further microstructuring experiments were performed with ultrashort pulses of a KrF excimer laser (wavelength: 248 nm, pulse duration: 0.5 ps, pulse energy: 10 mJ). This laser system was described in detail in [26]. The only difference from the former optical set-up was that the titanium sample disc and the focal point of the lens were situated inside a low-pressure (10 Pa) vacuum chamber equipped with a transparent fused silica (Suprasil) window. Vacuum conditions were necessary because of the high power density, in order to avoid optical breakdown in air. In these experiments, 1000 pulses with a fluence of 2.4 J/cm² were applied.

2.4. Microscopic investigations

The surface morphology of the samples was first observed through an optical microscope (Nikon Optiphot 100S metallurgical microscope). High-resolution secondary electron images were recorded with a scanning electron microscope (Hitachi S-2400). For a better visualisation of the structures in depth, all samples were tilted at 75° in SEM. For quantitative surface roughness determinations, AFM was applied (TopoMetrix Explorer TM, contact mode). The surface roughness characterised by the mean roughness (R_a) value was determined by using TopoMetrix software. R_a gives the average deviation of the surface height relative to the mean height.

2.5. X-ray photoelectron spectroscopy

One side of the titanium disk was polished by scanning over the whole surface area with laser pulses. The scanning speed was synchronised to the repetition rate of the laser, resulting in 10 overlapping laser shots with a fluence of 3.5 J/cm^2 . This sample was used for XPS and XRD investigations. The chemical composition of the titanium surfaces was studied by XPS. The photoelectrons generated by Al K_{α} primary radiation (14 kV, 15 mA) were analysed with a hemispherical electron energy analyser (Kratos XSAM 800). Binding energies were normalised with respect to the position of the C (1 s) peak. The changes in the XPS spectra were measured after 10 min of Ar^+ bombardment, repeated several times. Ar^+ was generated with an ion gun energy of 3 kV and the incident ion beam current density was $4\text{ }\mu\text{A/cm}^2$. Bombardment for 10 min removed about 10 nm from the surface of the material. Wide-range scans and higher-resolution narrow scans of the main characteristic peaks were recorded (Ti 2p, O 1s, and N 1s).

2.6. X-ray diffraction measurements

In order to compare the crystalline structures of the laser-treated samples with those of the non-irradiated materials XRD spectra were recorded, using Cu K_{α} radiation ($\lambda = 0.154\text{ nm}$). The XRD measurements were performed with a Philips PW 1830 X-ray generator (40 kV, 25 mA) with a powder diffractometer (PW 1877 Philips). The measured scan was taken between 2θ values of 20° and 80° , with a step size of 0.02° .

3. Results and discussion

3.1. Surface polishing

3.1.1. Microscopic analysis of laser-polished samples

ArF laser polishing was performed by applying 10 laser shots at a fluence of 1.5 J/cm^2 . The efficiency of the polishing improved as the fluence was increased from 1.5 to 5 J/cm^2 . As shown in the SEM micrograph in Fig. 1, the small scratches at intervals measuring $< 10\text{ }\mu\text{m}$, were completely eliminated in the machined samples. Larger structures were merely reduced in height, but not completely removed, which resulted in a wavy surface (Fig. 1b). Sample surfaces subjected to a higher number of shots (100 or 1000) exhibited undesired waves, holes and plate-like formations (Fig. 2).

The AFM surface topography pictures allowed a quantitative analysis of the surface roughness, as shown in Fig. 3. For the original machined samples, the roughness was $R_a = 256\text{ nm}$ (Fig. 3a). The surface roughness of the laser-polished samples irradiated with 10 laser pulses with a fluence of $\sim 5\text{ J/cm}^2$ was

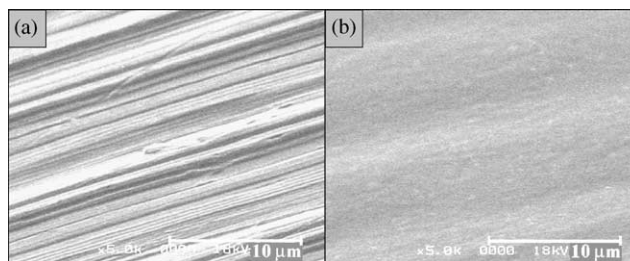


Fig. 1. SEM micrographs of: (a) non-irradiated machined and (b) ArF laser-polished titanium disk. The polishing was performed with 10 laser shots at a fluence of 3.5 J/cm^2 .

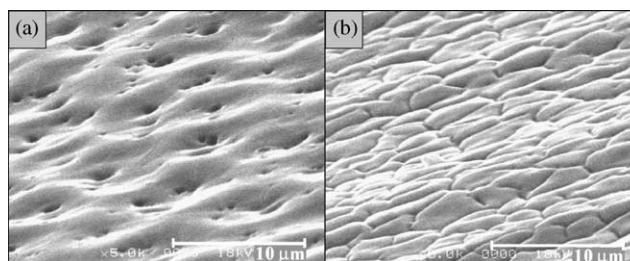


Fig. 2. SEM micrographs of structures formed on titanium surfaces illuminated with (a) 100 or (b) 1000 ArF laser shots at a fluence of 1.5 J/cm^2 .

significantly decreased, as revealed by the AFM micrographs (Fig. 3b): $R_a = 25\text{ nm}$. This value meets the requirements described in [27], where it was demonstrated that $R_a \leq 88\text{ nm}$ for a titanium surface is optimum for the inhibition of plaque accumulation and maturation.

Both the SEM and the AFM studies confirmed that a titanium sample with $R_a < \sim 1\text{ }\mu\text{m}$ can be effectively polished by homogeneous, $3\text{--}5\text{ J/cm}^2$ fluence laser illumination. Polishing can occur via several mechanisms. During the applied laser irradiation, the surface material melts and evaporates. This was confirmed by the appearance of laser-induced plasma during polishing. Prior to resolidification, the molten surface can become smoothed. Another mechanism is described in [20]: the absorbed laser light heats the emergent sharp peaks of the rough surface more efficiently than the valleys, where the heat diffusion is more effective. The result is more material removal on the hills, and finally the surface will be smoother.

3.1.2. XPS measurement of the surface chemistry

The XPS survey spectra illustrated in Fig. 4 confirmed the presence of oxygen, nitrogen and carbon on both non-irradiated and laser-treated samples. These elements are typically observed on titanium implant surfaces [28]. Trace amounts of phosphorus and chlorine could also be detected as in [29,30]. The upper part of Fig. 4 depicts spectra recorded without any Ar^+ sputter, while the lower part presents spectra after

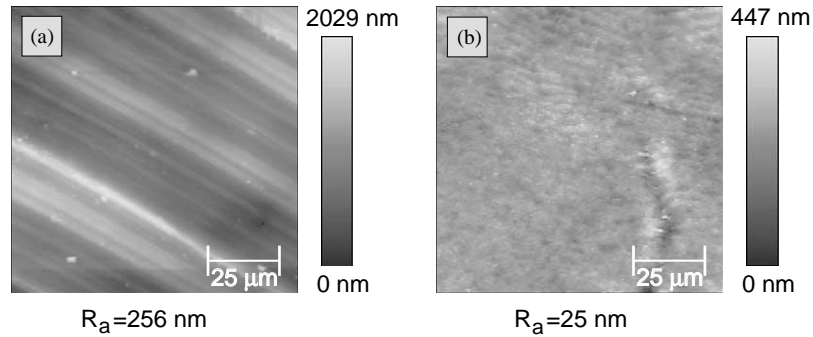


Fig. 3. AFM surface topography images of: (a) non-irradiated and (b) ArF laser-polished titanium disk. The polishing was performed with 10 laser shots at a fluence of 5 J/cm^2 . The surface roughness (R_a) for the non-irradiated and the laser-polished surface was 256 and 25 nm, respectively.

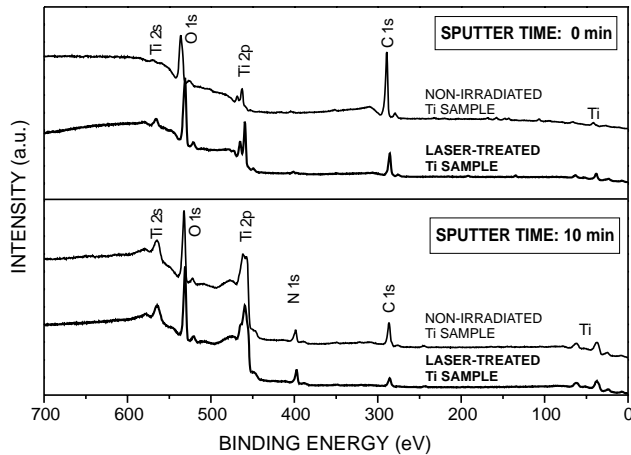


Fig. 4. XPS survey spectra of non-irradiated and ArF-laser polished (10 laser shots at 3.5 J/cm^2) titanium disks. Upper part: spectra recorded without Ar^+ sputter; lower part: spectra after 10 min of Ar^+ bombardment.

10 min of Ar^+ bombardment. In general, the laser treatment altered the surface chemistry in only a few respects. The substantial drop in the C 1s signal demonstrates that the excimer laser illumination effectively cleans the titanium surface. The C 1s signal indicates the presence of carbonaceous contamination, due to carbon-containing molecules remaining after chemical cleaning or adsorbed later on air-exposed surfaces [30,31].

Representative high-resolution Ti 2p spectra of non-irradiated and laser-treated titanium samples after 10, 20 and 30 min of Ar^+ sputtering are shown in Fig. 5. The core level spectra after a single Ar^+ bombardment are similar, with three characteristic peaks, at 464.7, 459 and 455.6 eV. The positions of the Ti 2p_{1/2} and Ti 2p_{3/2} peaks correspond to those measured in TiO_2 [32]. The shoulder appearing at the lowest binding energy can be assigned to Ti 2p_{3/2} in TiN [33]. This reveals that, besides a thin TiO_2 layer, TiN impurities (probably originating from the basic material [34]) are also present on the sample surface. The presence of N was supported by the concomitant increment of the N 1s peak during

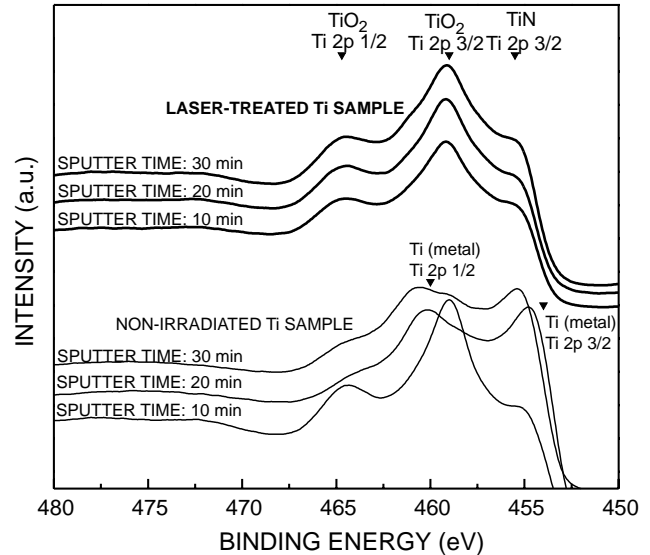


Fig. 5. High-resolution XPS spectra showing Ti 2p lines of non-irradiated and ArF laser-treated titanium samples (after 10, 20 and 30 min of Ar^+ sputtering).

Ar^+ sputtering. This can also be seen from a comparison of the curves corresponding to sputtering times of 0 and 10 min in Fig. 5.

It is interesting to compare the spectra in Fig. 5 that were measured after a second and a third Ar^+ sputter. The spectrum of the non-irradiated titanium surface includes peaks at binding energies of around 460 and 454 eV, corresponding to pure Ti metal [33,35], while that of the laser-treated sample still exhibits the group of three peaks indicating the oxidised state of titanium as mentioned above, even after the second and third Ar^+ bombardments. Consequently, laser-polishing thickens the oxide layer at least 2-fold, which may favour the use of laser techniques to achieve better osseointegration [13].

3.1.3. XRD analysis

Rapid laser annealing by a series of ns laser pulses may alter the crystalline structure of the implant in the heat-affected zone. At room temperature the hexagonal

α form of titanium is stable, while above 1158 K this phase changes to cubic β -titanium. It is essential to preserve the original crystal structure of the implant in order to avoid stress formation in it. The changes in crystal structure were followed by comparing the XRD spectra of the non-irradiated and laser-polished probes (Fig. 6). The XRD spectrum of the non-irradiated probe mainly shows the peaks of α -titanium [24,36], but the peaks at $2\theta = 31.61^\circ, 34.59^\circ, 36.13^\circ, 47.53^\circ$ and 56.29° demonstrate that other crystalline form(s) are present as well. Diffraction peaks at 34.59° and 38.42° can be attributed to surface contamination, since laser treatment resulted in significant decreases in intensity of these peaks. The XRD spectrum of the laser-polished probe reveals the intensity characteristics of pure α -titanium [37], indicated at the bottom of Fig. 6. The origins of the non- α -titanium peaks in the non-irradiated probes have not yet been clarified. The increase in the peak measured at 38.42° for the non-irradiated probe might possibly be assigned to the strong diffraction at 38.48° originating from the (110) plane of β -titanium, but this assumption cannot be true, since other peaks characteristic of β -titanium (e.g. at 55.54° and 69.60°) are completely missing from both diffraction curves. Titanium oxides such as anatase or rutile cannot furnish these non- α -titanium peaks either, because other strong characteristic titanium oxide peaks are absent from the spectra (e.g. the highest-intensity peaks at 25.32° and 27.37° , respectively, for anatase and rutile [36]). Diffraction peaks of crystalline nitrides or carbides of titanium [38,39] can likewise not be

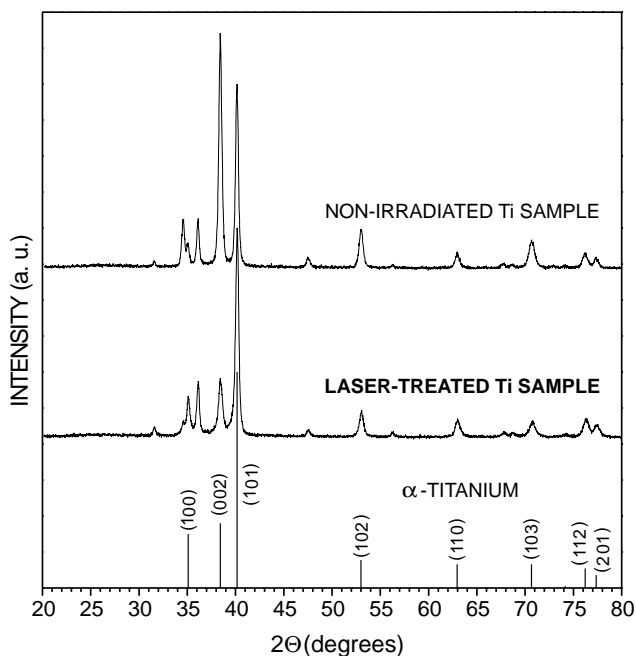


Fig. 6. XRD spectra of non-irradiated and ArF laser-polished probes. The relative intensities of pure α -titanium are indicated at the bottom.

correlated with these locations. These diffraction peaks probably originate from crystalline forms of non-stoichiometric titanium compounds, e.g. oxides, nitrides or carbides, which were indicated by XPS. As X-ray diffraction is a bulk technique, it is naturally not possible to exclude with certainty the presence of a thin layer of some other material with a crystalline or amorphous structure. As concerns applicability, we can conclude that laser treatment results in cleaning of the surface and maintenance of the crystal structure of the titanium probe in α form.

3.2. Microstructuring

3.2.1. Surface patterning by ns excimer pulses

Holes at a characteristic distance of about $25\ \mu\text{m}$ from each other were successfully ablated into the titanium surface by imaging a grid with ArF excimer laser pulses, as revealed by the SEM images in Figs. 7a and b. The surface was ablated locally at those sites where the fluence exceeded the ablation threshold. Increase of the number of pulses led to the ablation of holes with a higher aspect ratio. At the same time, rims formed around the edges of the holes as can be seen in Figs. 7a and b. After 250 shots at a fluence of $8.5\ \text{J}/\text{cm}^2$, the depth of the holes was about $10\ \mu\text{m}$ and the height of the rims was at most $8\ \mu\text{m}$. From the depth of the ablated holes, the effective evaporated thickness proved to be approximately $40\ \text{nm}$ per pulse. Formation of the separate craters was possible because the heat diffusion length (for a pulse duration of 18 ns this is $\sim 800\ \text{nm}$ for titanium) was shorter than the distance between the holes.

In nature, the holes resemble the drilled patterns made by other pulsed laser sources (e.g. Nd:YAG lasers) operated at longer wavelengths [23]. The temperature distribution in metals is determined mostly by the heat conduction and not by the wavelength-dependent absorption. The absorption penetration depths at 193, 248 and $1064\ \text{nm}$ are 13.5, 12.7, and $253.3\ \text{nm}$, respectively. These values are 1–2 orders of magnitude smaller than the above-mentioned heat diffusion length. It is common in these techniques that the ablation occurs via extensive evaporation and melting. In the applied

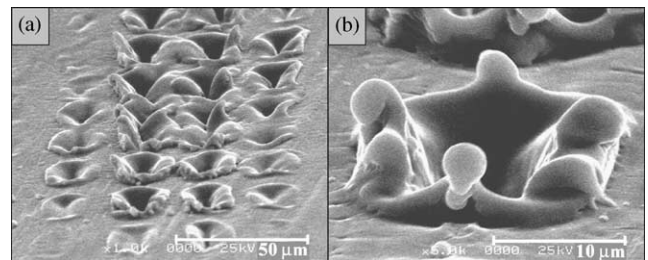


Fig. 7. SEM micrographs at different magnifications of ablated holes formed in a titanium surface after 250 shots of the ArF excimer laser. The fluence applied was $8.5\ \text{J}/\text{cm}^2$.

fluence range, plasma is formed and the underlying molten layer is propelled out as a radial hydrodynamic flow due to the high recoil plasma pressures. During this process, rims are formed at the edges [23]. This is an inconvenient effect, since the rims may break away from the implant surface during the implanting procedure and contaminate the surrounding biological tissues.

3.2.2. Surface patterning by sub-ps excimer pulses

The debris-free processing of holes with high aspect ratios, which are commonly produced in the short-wavelength excimer laser ablation of specific polymers and ceramics, cannot be reproduced in the case of metals with relatively high thermal conductivities. Similarly as in drilling with ns length pulses of Q-switched Nd:YAG lasers, at an excimer pulse duration of 18 ns, the heat-affected zone is defined by the thermal diffusion length and not by the absorption penetration depth of the laser light. In this case the molten depth may approach 1 μm and the melt flows out from the high-pressure zones of high-temperature laser plasma. One possibility to overcome the problems of rim formation is to decrease the extent of heat diffusion. The application of 0.5 ps laser pulses allows a heat diffusion length of 4.3 nm. In this case the absorption penetration depth will determine the precision of laser processing. A number of authors have investigated the pulse duration requirements for the melting- and burr-free drilling of metals [20,40–44]. The highest process efficiency and hole quality can be achieved by using sub-ps pulse durations. On repetition of the surface patterning experiments with a 0.5 ps KrF excimer laser, rim formation could be eliminated completely, as illustrated in the SEM micrograph in Fig. 8. The laser fluence here was 2.4 J/cm² and 1000 shots had to be administered.

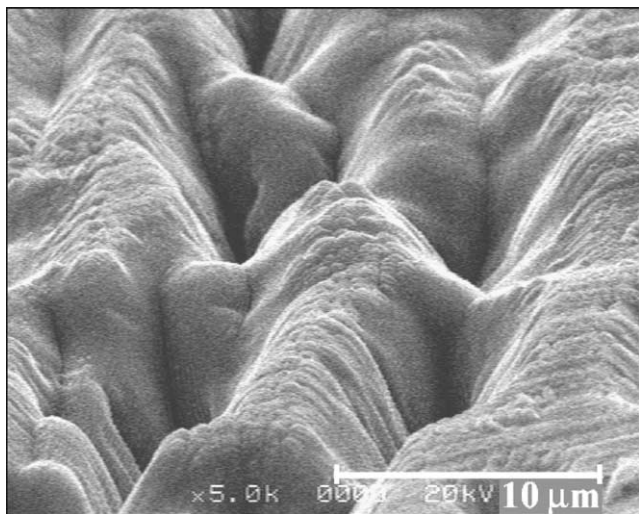


Fig. 8. SEM micrograph of ablated holes formed in a titanium surface after 1000 shots of the 0.5 ps KrF excimer laser. The fluence applied was 2.4 J/cm².

The coherence properties of the applied 0.5 ps laser system led to less accurate imaging of the mask pattern on the sample surface. The topography of the ablated structure practically reproduces the intensity distribution in the image plane, which is distorted by interference phenomena. Accordingly, the ablated holes do not possess sharp and well-defined borders. The aspect ratio of the holes is sufficient for the required purpose, since the contact interface of the osseointegrating tissues was enlarged significantly.

4. Conclusions

The chemical composition and morphology of the titanium surface were modified by excimer laser processing. Effective polishing was achieved by homogeneous illumination with ns laser pulses in the 3–5 J/cm² fluence range, as revealed by SEM and AFM studies. Carbonaceous contamination was removed, as indicated by XPS and XRD measurements, demonstrating that polishing with an excimer laser cleans the surface of titanium. The XRD data confirmed that the laser polishing process did not alter the original crystalline structure, while the XPS measurements proved that pulsed laser oxidation in air resulted in an increased thickness of the surface oxide layer.

Holes about 20 μm diameter and 10 μm in depth with rims around the edges were ablated into the titanium surface with pulses of ns ArF excimer laser. To avoid the formation of these fragile rims, we applied an excimer pulse duration of 0.5 ps, whereby the melting- and rim-free ablation of titanium was attained.

Acknowledgements

The authors thank Albert Oszkó from the Department of Solid-State and Radiochemistry at the University of Szeged for the XPS measurements, Dr. Ágnes Patzkó from the Department of Colloid Chemistry at the University of Szeged for the XRD measurements, and Prof. Sándor Szatmári for providing access to the 0.5 ps KrF laser facility at the Department of Experimental Physics, University of Szeged. The optical microscope used was purchased with World Bank—OTKA support (OTKA-W015254).

References

- [1] Williams DF. Implants in dental and maxillofacial surgery. *Biomaterials* 1981;2:133.
- [2] Lemons JE. Dental implant biomaterials. *J Am Dent Assoc* 1990;121:716–9.
- [3] Craig RG. In: Powers JM, Craig RG, editors. *Restorative dental materials*. St. Louis: Mosby Inc.; 1989. p. 169.

- [4] Meffert RM, Langer B, Fritz ME. Dental implants: a review. *J Periodontol* 1992;63:859–70.
- [5] Brånemark PI, Adell R, Albrektsson T, Lekholm U, Lundkvist S, Röckler B. Osseointegrated titanium fixtures in the treatment of edentulousness. *Biomaterials* 1983;4:25–8.
- [6] Albrektsson T. The response of bone to titanium implants. *CRC Crit Rev Biocompat* 1985;1:53.
- [7] Lautenschlager EP, Monaghan P. Titanium and titanium alloys as dental materials. *Int Dental J* 1993;43:245–53.
- [8] Michel R. Trace metal analysis in biocompatibility testing. *CRC Cri Rev Biocompat* 1987;3:235.
- [9] Binon PP, Weir DJ, Marshall SJ. Surface analysis of an original Brånemark implant and three related clones. *Int J Oral Max Implants* 1992;7:168–75.
- [10] Olefjord I, Hansson S. Surface analysis of four dental implant systems. *Int J Oral Max Implants* 1993;8:32–40.
- [11] Cochran DL. A comparison of endosseous dental implant surfaces. *J Periodontol* 1999;70:1523–39.
- [12] Uitto VJ, Larjava H, Peltonen J, Brunette DM. Expression of fibronectin and integrins in cultured periodontal-ligament epithelial-cells. *J Dent Res* 1992;71:1203–11.
- [13] Eriksson C, Lausmaa J, Nygren H. Interactions between human whole blood and modified TiO₂-surfaces: influence of surface topography and oxide thickness on leukocyte adhesion and activation. *Biomaterials* 2001;22:1987–96.
- [14] Buser D, Schenk RK, Steinmann S, Fiorellini JP, Fox CH, Stich H. Influence of surface characteristics on bone integration of titanium implants—a histomorphometric study in miniature pigs. *J Biomed Mater Res* 1991;25:889–902.
- [15] Wong M, Eulenberger J, Schenk R, Hunziker E. Effect of surface-topology on the osseointegration of implant materials in trabecular bone. *J Biomed Mater Res* 1995;29:1567–75.
- [16] Wennerberg A, Ektessabi A, Albrektsson T, Johansson L, Andersson B. A 1-year follow-up of implants of differing surface roughness placed in rabbit bone. *Int J Oral Max Implants* 1997;12:486–94.
- [17] Boyan BD, Batzer R, Kieswetter K, Liu Y, Cochran DL, Szmuckler-Moncler SS, Dean DD, Schwartz Z. Titanium surface roughness alters responsiveness of MG63 osteoblast-like cells to 1 alpha,25-(OH)(2)D-3. *J Biomed Mater Res* 1998;39:77–85.
- [18] Hansson H, Albrektsson T, Brånemark PI. Structural aspects of the interface between tissue and titanium implants. *J Prosth Dent* 1983;50:108–13.
- [19] Quirinen M, Bollen CM, Papaioannou W, Van Eldere J, van Steenberghe D. The influence of titanium abutment surface roughness on plaque accumulation and gingivitis: short-term observations. *Int J Oral Max Implants* 1996;11:169–78.
- [20] Bäuerle D. *Laser processing and chemistry*. Berlin, Heidelberg, New York, Tokyo: Springer; 2000.
- [21] Gaggi A, Schultes G, Müller WD, Kärcher H. Scanning electron microscopical analysis of laser-treated titanium implant surfaces—a comparative study. *Biomaterials* 2000;21:1067–73.
- [22] Pető G, Karacs A, Pászti Z, Gucci L, Divinyi T, Joób A. Surface treatment of screw shaped titanium dental implants by high intensity laser pulses. *Appl Surf Sci* 2001;7524:1–7.
- [23] György E, Mihailescu IN, Serra P, Pérez del Pino A, Morenza JL. Crown-like structure development on titanium exposed to multiple NdYAG laser irradiation. *Appl Phys A* 2002;74:755–9.
- [24] Perez del Pino, Serra P, Morenza JL. Oxidation of titanium through Nd:YAG laser irradiation. *Appl Surf Sci* 2002;197–198:887–90.
- [25] Nánai L, Vajtai R, George TF. Laser-induced oxidation of metals: state of art. *Thin Solid Films* 1997;298:160–4.
- [26] Szatmari S, Schäfer FP. Simplified laser system for the generation of 60 fs pulses at 248 nm. *Opt Commun* 1988;68:196–202.
- [27] Rimondini L, Faré S, Brambilla E, Felloni A, Consonni C, Brossa F, Carrassi A. The effect of surface roughness on early in vivo plaque colonization on titanium. *J Periodontol* 1997;68:556–62.
- [28] Ameen AP, Short RD, Johns R, Schwach G. The surface analysis of implant materials 1. The surface composition of a titanium dental implant material. *Clin Oral Implants Res* 1993;4:144–50.
- [29] Brånemark PI, Zarb GA, Albrektsson T. *Gewebeintegrierter zahnersatz*. Berlin, Chicago, London, Rio de Janeiro, Tokio: Quintessenz Verlags-GmbH; 1985. p. 109–11.
- [30] Lausmaa J, Kasemo B. Surface spectroscopic characterization of titanium implant materials. *Appl Surf Sci* 1990;44:133–46.
- [31] Sawase T, Hai K, Yoshida K, Baba K, Hatada R, Atsuta M. Spectroscopic studies of three osseointegrated implants. *J Dent* 1998;26:119–24.
- [32] Kilpadi DV, Raikar GN, Liu J, Lemons JE, Vohra Y, Gregory JC. Effect of surface treatment on unalloyed titanium implants: spectroscopic analyses. *J Biomed Mater Res* 1998;40:646–59.
- [33] NIST XPS Database, 2000 (<http://srdata.nist.gov/xps>).
- [34] Park JY, Gemmell CH, Davies JE. Platelet interactions with titanium: modulation of platelet activity by surface topography. *Biomaterials* 2001;22:2671–82.
- [35] Arys A, Philippart C, Dourov N, He Y, Le QT, Pireaux JJ. Analysis of titanium dental implants after failure of osseointegration: combined histological, electron microscopy, and X-ray photoelectron spectroscopy approach. *J Biomed Mater Res* 1998;43:300–12.
- [36] Sul YT, Johansson CB, Petronis S, Krozer A, Jeong Y, Wennerberg A, Albrektsson T. Characteristics of the surface oxides on turned and electrochemically oxidized pure titanium implants up to dielectric breakdown: the oxide thickness, micropore configurations, surface roughness, crystal structure and chemical composition. *Biomaterials* 2002;23:491–501.
- [37] Sailer R, McCarthy G. ICCD grant-in-aid. North Dakota, USA: Fargo; 1993.
- [38] Voevodin AA, Capano MA, Laube SJP, Donley MS, Zabinski JS. Design of a Ti/TiC/DLC functionally gradient coating based on studies of structural transitions in Ti–C thin films. *Thin Solid Films* 1997;298:107–15.
- [39] Zehnder T, Patscheider J. Nanocomposite TiC/a–C:H hard coatings deposited by reactive PVD. *Surf Coatings Technol* 2000;133–134:138–44.
- [40] Kruger J, Kautek W. The femtosecond pulse laser: a new tool for micromachining. *Laser Phys* 1999;9:30–40.
- [41] Banks PS, Feit MD, Rubenchik AM, Stuart BC, Perry MD. Material effects in ultra-short pulse laser drilling of metals. *Appl Phys A* 1999;69:S377.
- [42] Zhu X, Naumov AY, Villeneuve DM, Corkum PB. Influence of laser parameters and material properties on micro drilling with femtosecond laser pulses. *Appl Phys A* 1999;69:S367–71.
- [43] Tonshoff HK, Momma C, Ostendorf A, Nolte S, Kamlage G. Microdrilling of metals with ultrashort laser pulses. *J Laser Appl* 2000;12:23–7.
- [44] Békési J, Klein-Wiele JH, Simon P. Efficient submicron processing of metals with femtosecond UV pulses. *Appl Phys A* 2003;76:355–7.